

## Quantifying the A<sub>1</sub>AR distribution in peritumoural zones around experimental F98 and C6 rat brain tumours

Markus Dehnhardt · Christoph Palm ·  
Andrea Vieten · Andreas Bauer · Uwe Pietrzyk

Received: 25 February 2007 / Accepted: 6 April 2007 / Published online: 12 May 2007  
© Springer Science+Business Media B.V. 2007

**Abstract** Quantification of growth in experimental F98 and C6 rat brain tumours was performed on 51 rat brains, 17 of which have been further assessed by 3D tumour reconstruction. Brains were cryosliced and radio-labelled with a ligand of the peripheral type benzodiazepine-receptor (pBR), <sup>3</sup>H-Pk11195 [(1-(2-chlorophenyl)-N-methyl-N-(1-methyl-propylene)-3-isoquinoline-carboxamide)] by receptor autoradiography. Manually segmented and automatically registered tumours have been 3D-reconstructed for volumetric comparison on the basis of <sup>3</sup>H-Pk11195-based tumour recognition. Furthermore automatically computed areas of ~300 µm inner (marginal) zone as well as 300 µm and 600 µm outer tumour space were quantified. These three different regions were transferred onto other adjacent slices that had been labelled by receptor autoradiography with the A<sub>1</sub> Adenosine receptor (A<sub>1</sub>AR)-ligand <sup>3</sup>H-CPFPX (<sup>3</sup>H-8-cyclopentyl-3-(3-fluorpropyl)-1-propylxanthine) for quantitative assessment of A<sub>1</sub>AR in the three different tumour zones. Hence, a method is described for quantifying various receptor protein systems in the tumour as well as in the marginal invasive zones around

experimentally implanted rat brain tumours and their representation in the tumour microenvironment as well as in 3D space. Furthermore, a tool for automatically reading out radio-labelled rat brain slices from auto radiographic films was developed, reconstructed into a consistent 3D-tumour model and the zones around the tumour were visualized. A<sub>1</sub>AR expression was found to depend upon the tumour volume in C6 animals, but is independent on the time of tumour development. In F98 animals, a significant increase in A<sub>1</sub>AR receptor protein was found in the Peritumoural zone as a function of time of tumour development and tumour volume.

**Keywords** 3D reconstruction · A<sub>1</sub> adenosine receptor · GBM · K<sub>means</sub> algorithm · Brain tumour · Receptor autoradiography

### Abbreviations

A <sub>1</sub> AR	A <sub>1</sub> adenosine receptor
C6	Cloned rat glial tumour cell line
CPFPX	8-Cyclopentyl-3-(3-fluorpropyl)-1-propylxanthine)
F98	Astrocytic tumour cell line
GBM	Glioblastoma multiforme
Pk11195	1-(2-chlorophenyl)-N-methyl-N-(1-methyl-propylene)-3-isoquinoline-carboxamide
pBR	Peripheral-type benzodiazepine receptor
R-PIA	(R(-)-N-(2-phenylisopropyl)-adenosine

Markus Dehnhardt and Christoph Palm contributed equally to the manuscript.

M. Dehnhardt (✉) · C. Palm · A. Vieten ·  
A. Bauer · U. Pietrzyk  
Institute of Neuroscience and Biophysics 3-Medicine, Research  
Centre Juelich, 52425 Juelich, Germany  
e-mail: m.dehnhardt@medac.de

### Present Address:

M. Dehnhardt  
Medac GmbH, Theaterstr. 6, 22880 Wedel, Germany

### Present Address:

C. Palm  
Centre for Medical Image Computing (CMIC), University  
College London, London, United Kingdom

### Introduction

We have recently shown that the density of A<sub>1</sub> adenosine receptors (A<sub>1</sub>AR) is increased in a zone surrounding

experimental tumours and human glioblastoma multiforme (GBM) [1]. It is likely that the A<sub>1</sub>AR is an indicator of processes related to local tumour infiltration. To follow A<sub>1</sub>AR changes with selective radioprobes and positron emission tomography could, therefore, provide a new means to study tumour invasion non-invasively. This will become of particular importance for the development of immunomodulatory anti-tumour strategies. In order to evaluate the proposed method it is important to understand the patho-physiological background of the observed receptor changes, particularly, whether A<sub>1</sub>AR expression could hold as a prognostic marker, reflects a certain tumour developmental stage or ~size or occurs only in certain zones of the tumour microenvironment.

As has been described elsewhere [2, 3], tumours from human GBM species or of comparable implantation models show varying microenvironments or zonal organization as a function of their origin or size [4], e.g. a peritumoural zone, the solid tumour and a central area. Various treatment options might be derived from spatial differences in protein expression pattern [2], blood vessel supply [5] or occurrence of hypoxic events, especially with increasing size leading to HIF expression and induction of a broad spectrum of related genes [6, 7].

Among solid tumours, the A<sub>1</sub>AR has been shown to be present in the environment of colon carcinomas [8] and holds as a promising marker of the peritumoural zone in primary GBM [1].

As GBM reach considerable sizes within short time intervals and expand within various brain nuclei or functional entities that show different levels of A<sub>1</sub>AR themselves (e.g. cortex, hippocampus, thalamus) [9], the availability of free adenosine within these regions of tumour growth can be different as well as the occupancy of A<sub>1</sub>AR.

It is obvious that appropriate tools are warranted that have the capability to quantify protein expression in the tumour 3D space and to display different proteins or elements in the meantime spatially.

With respect to different spatial zones in and around tumours over time, in the present paper a qualitative and quantitative analysis was made of the possible inhomogeneous distribution of spatial A<sub>1</sub>AR and pBR expression in and around experimentally implanted brain-tumours.

### Experimental paradigm

In order to meet these needs, a semi-automatic tool has been developed for 3D quantitation of tumour growth, size and shape from rat brain tumour models of the F98 [10] and the C6 [11] astrocytic tumour cell lines.

The growth of F98 tumours of 100 or 1000 tumour cells implanted in the caudate putamen (CPU) of male Fisher rats and of 1000 or 10,000 C6 tumour cells implanted in the CPU of Wistar rats was quantified as a factor of the length

of time of tumour development (10, 14, 18 and 20 days, respectively), as a factor of implanted tumour cells, as well as of the volume of the tumour entity.

Following cryostat slicing of the entire brain tumour after 10, 14, 18 and 20 days of tumour growth, respectively, adjacent slices were subjected to either receptor auto radiography protocols for A<sub>1</sub>AR or pBR, or were stained histologically by cresylene-violet for cell body labelling, whereas the following slice was used in immuno-histochemistry. Hence, each fourth slice was labelled following the same protocol.

In the present study, both ligands, <sup>3</sup>H-Pk11195 as well as <sup>3</sup>H-CPFPX, have been used for labelling the tumour and peritumoural zone, respectively, in adjacent cryoslices from the same animal. It was decided to use the *post mortem* rather than the *ex vivo* technique to avoid disturbing the <sup>3</sup>H-CPFPX-binding by the possible presence of endogenous adenosine.

The quantification of the tumour size was finally achieved by manual segmentation of the outer tumour border following <sup>3</sup>H-Pk11195 labelling. Around the tumour border, three different zones were automatically labelled using Euclidean distance mapping [12]. Therefore, computed areas of ~300 µm inner (marginal) zone as well as 300 µm and 600 µm outer tumour space were quantified and were automatically retransferred onto adjacent <sup>3</sup>H-CPFPX-labelled slices in a specific auto radiographic software program, AIDA<sup>®</sup> (Raytest, Straubenhardt, Germany). By superimposition with the <sup>3</sup>H-CPFPX-labelled slice that was at maximum two slices away from the <sup>3</sup>H-PK11195-labelled one, the quantitative zonal A<sub>1</sub>AR-distribution was screened.

Rostro-caudal A<sub>1</sub>AR-expression differences were assessed in 3D based on the automatic rigid restacking of the Pk labelling. Regarding the A<sub>1</sub>AR, analogous restacking of the various zones was done with layer-averaged <sup>3</sup>H-CPFPX-values. The merged visualization of brain, tumour and zones was performed with AMIRA<sup>®</sup> visualization software (Mercury Computer Systems, Berlin, Germany).

## Methods

### Animals

Animals were housed in a 12-h light-dark cycle with food and water *ad libitum* and treated according to the ethics and guidelines of the German federal law on animal care and the guidelines of the federal state of North Rhine-Westphalia (Fisher and Wistar rats), with experimental procedures approved by an ethics commission of 12/2003. For experimental procedures with F98 tumours, only male Fisher rats were used, whereas for procedures employing C6 tumour cells, male Wistar rats were used (both strains from Charles River, Sulzfeld, Germany) both 150–200 g in weight and approximately 1.5 years of age.

## Implantation of tumours

In order to implant tumour cells into the right caudate putamen, animals were anaesthetized with a mixture of ketamine/xylazine (100 mg/kg and 10 mg/kg body weight,

i.p.) and placed in a stereotaxic frame (from David Kopf Instruments, Tujunga, California, USA). Following removal of the scalp, a  $\varnothing$  0.8 mm hole was drilled with a commercial dentist's driller above the target coordinates [AP:  $-2.5$ , ML:  $2.0$ , DV:  $-5.0$ mm] (Fig. 1). Tumour

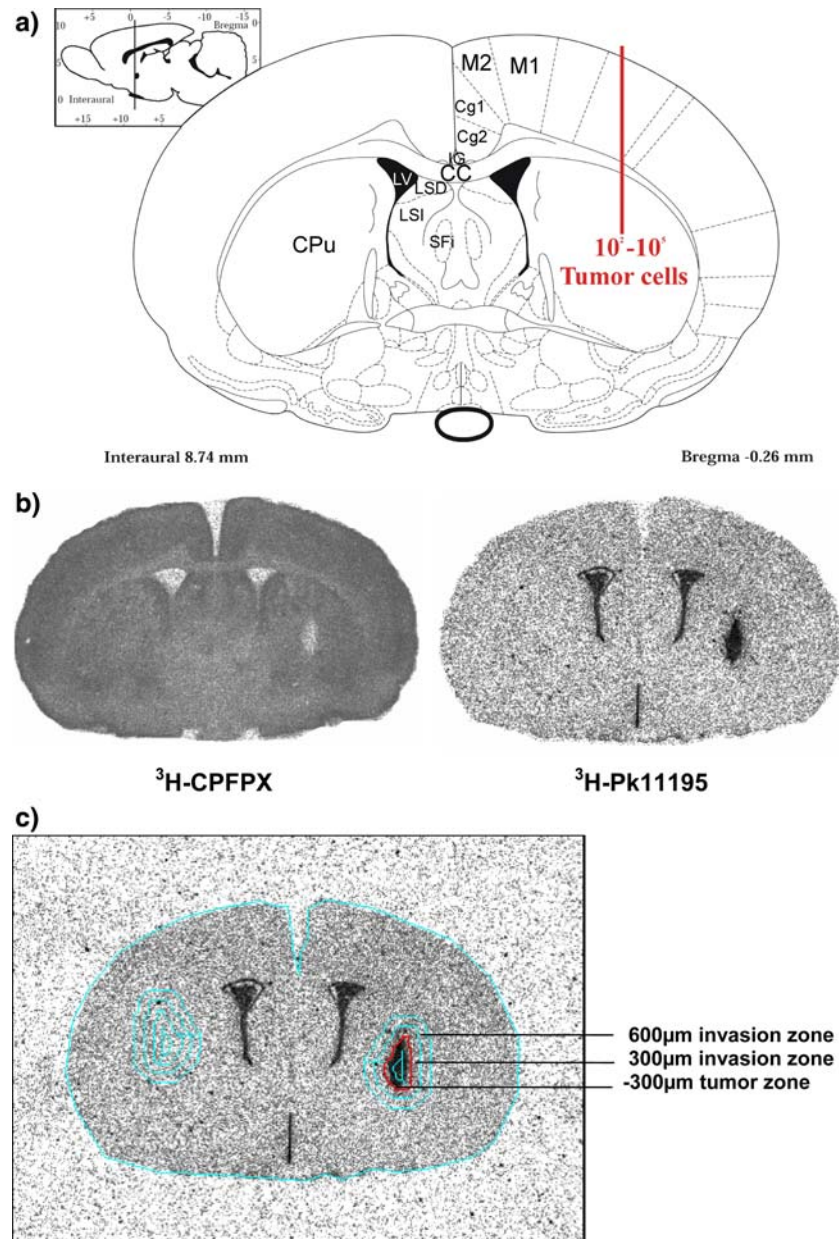


**Fig. 1** (a) Implantation of tumour cells. Implantation scheme. Stereotaxically guided tumour implantation by injection of  $5 \mu\text{l}$   $10^2$  to  $10^4$  F98 cells into the right caudate putamen. Target coordinates are AP:  $-2.5$ , ML:  $2.0$ , DV:  $-5.0$  mm with respect to bregma [18]. (b) Autoradiograph of a section through a rat telencephalic nuclei labelled with  $^3\text{H}$ -Pk11195 ([ $^3\text{H}$ -(1-(2-chlorophenyl)-N-methyl-N-(1-methylpropyl)-3-isoquinoline-carboxamide)]) a pBR ligand at  $1 \text{ pM}$  (right-hand side), and of an adjacent slice labelled with  $^3\text{H}$ -CPPFX ([ $^3\text{H}$ ]8-cyclopentyl-3-(3-fluoropropyl)-1-propylxanthin) at a concentration close to half-maximal binding ( $4 \text{ nM}$ , left-hand side). (c) Explanation of the various zones assessed in tumours. The outer

tumour border is outlined in red. Relative to this, an inner  $-300 \mu\text{m}$  zone, and two outer zones ( $0$  to  $300 \mu\text{m}$  and  $300$  to  $600 \mu\text{m}$ ) are determined on the basis of  $25 \mu\text{m}$  pixel resolution of the receptor autoradiographic technique. We refer to these zones as the  $300 \mu\text{m}$  tumour zone,  $300 \mu\text{m}$  peritumoural zone and  $600 \mu\text{m}$  peritumoural zone. *Abbreviations:* M1, primary motor cortex; M2, secondary motor cortex; Cg1, cingulate cortex area 1; Cg2, cingulate cortex area 2; IG, indusium griseum; CC, corpus callosum; LSD, lateral septal nucleus (dorsal part); LSI, lateral septal nucleus (intermediate); Sfi, septo-fimbrial nucleus; LV, lateral ventricle; CPU, caudate putamen

implantation was stereo-tactically guided and performed by injecting  $5 \mu\text{l}$   $10^2$  to  $10^4$  tumour cells into the right caudate putamen with a Hamilton syringe. Following the implantation procedure, animals were treated with a wound and skin antiseptic (B. Braun, Melsungen, Germany) and analgesics (Metoxicam, 0.2 mg/kg, Boehringer Ingelheim, 88400 Biberach an der Riss, Germany). During the time the animals were bearing the tumour, body weight, shape of the skull and overall behaviour was assessed daily. None of the animals showed any devastation or weight loss during the 20 days of experiments.

As first orienting experiments, double determinations with 1000 and 10000 cells (C6) and 100 and 1000 cells (F98) were tested in advance for appropriate estimation of growth kinetics and possible endpoints.

#### Tumour cells and in vitro procedures

C6 cells were obtained from American Type Culture Collection, ATCC, Manassas, VA, USA. Cells were cultured in 5%  $\text{CO}_2$ , 1% penicillin/ streptomycin, 15% horse serum, 2.5% foetal calf serum, 2 mM glutamine in Kaighn's modification of Ham's F12 medium (F12K). F98 cells were also obtained from ATCC and cultured in ATCC complete growth medium: Dulbecco's modified Eagle's medium with 4 mM L-glutamine, 1.5 g/l sodium bicarbonate and 4.5 g/l glucose (90%), 10% foetal bovine serum (FBS), temperature: 37°C atmosphere: air, 95%; carbon dioxide ( $\text{CO}_2$ ), 5%.

For sub-cultivation, cells were rinsed with 0.05% (w/v) 0.53 mM trypsin-EDTA solution to remove all traces of serum that contains trypsin inhibitor, and 2.0 to 3.0 ml of trypsin-EDTA solution was added. Cells were observed under an inverted microscope until the cell layer was dispersed (usually within 5 to 15 min). Following this, 6.0 to 8.0 ml of complete growth medium was added and the cells were aspirated by pipetting gently. A subcultivation ratio of 1:6 to 1:10 was followed as recommended. The medium was changed every 2–3 days. Cells were kept in culture to approximately 80% confluency and passaged. Only passages of C6 cells between passage 38 and 55 and passages of F98 cells between 20 and 30 were used for experimental procedures. The tumour cells were not synchronized before implantation. In order to assess the immunogenic components during tumour growth as well as events following traumatic events, two groups of animals with attenuated tumour cells were used. For attenuation, cells were resuspended in complete medium, centrifuged, and the pellet resuspended in 70% ethanol. Following storage for 24 h at  $-20^\circ\text{C}$  and a further washing step, the pellet was resuspended in complete medium for implantation.

#### RT-PCR

A quantity of 3  $\mu\text{g}$  of rat brain mRNA and isolated total F98- and C6-cell mRNA was transcribed into cDNA in a volume of 50  $\mu\text{l}$  using random hexanucleotide primers and Superscript<sup>TM</sup> reverse transcriptase (Invitrogen, Karlsruhe, Germany). As primers for  $\text{A}_1\text{AR}$  amplification, the forward primer sequence nt 61–83 (5'-tgctacattggcgcgaggtg) and the reverse primer sequence nt 959–980 (5'-catcgatggaggcttaggctg) were used, yielding a PCR product of 919 bp. As a control for the cell lines, the amount of cDNA was controlled by assessing the expression of calmodulin by RT-PCR, yielding a transcript product of 450 bp. Cycles consisted of 20 s of denaturation at  $94^\circ\text{C}$ , 20 s of annealing at  $62^\circ\text{C}$  and 60 s of elongation at  $72^\circ\text{C}$ , with 40 cycles performed. RT-PCR products were separated 2% agarose gels, and the ethidium bromide stained bands were recorded by the Gel-Doc 1000 system (Bio-Rad).

#### Sectioning of the rat tumour brains

After 10–20 days, the brains were removed, frozen in  $-50^\circ\text{C}$  N-methylene-butane and in a Leica 3010 cryostat cut into 20  $\mu\text{m}$  thick coronal slices at  $-20^\circ\text{C}$ . Sections were sampled from the beginning of the tumour up to the last slice containing the tumour.

Coronal sections were separated into four sets for staining, whereby the first consecutive slice was subjected to  $^3\text{H}$ -CPFPX autoradiography, the second to cresylene-violet staining, the third to  $^3\text{H}$ -Pk11195 autoradiography, the fourth to immunofluorescent stains (repetitively) until macroscopically the complete tumour was sectioned (as indicated by fast methylene blue stain and light microscopy). For this study, only CPFPX and Pk are processed further. Complete labelling/staining of the tumour was done for later 3D-reconstruction. 20- $\mu\text{m}$ -thick human GBM resections were treated accordingly.

#### Autoradiography

Autoradiography was performed by the slice preparation method as described elsewhere [1]. In brief, tumour sections on glass cover slips were dried in a stream of cold air and either stored in evacuated plastic bags at  $-80^\circ\text{C}$  for later processing or directly subjected to autoradiographic procedures. The slices were exposed to a ligand for the pBR protein that is up-regulated in the brain only under pathological conditions such as tumours,  $^3\text{H}$ -Pk11195 (100 pM) [(1-(2-chlorophenyl)-N-methyl-N-(1-methylpropyl)-3-isoquinoline-carboxamide)] [13]. Non-specific binding was determined with slices on which the tritiated ligand was competed with an excess of unlabelled sample, cold Pk11195. Alternatively, slices were autora-

diographed with  $^3\text{H}$ -CPFPX, a specific marker for  $\text{A}_1\text{AR}$  ( $\text{A}_1\text{AR}$ ) at 4.4 nM, which has been reported recently as a marker for invasive zones of tumours in rat studies as well as in human high-grade glioma patients [1].

### Image acquisition

Radiolabelled slices were exposed for 3 days to a tritium-sensitive film plate (Fuji Inc., Tokyo, Japan). Autoradiographic images were obtained from a Bas reader and AIDA software (Raytest, Straubenhardt, Germany) with a spatial resolution of 25  $\mu\text{m}$ . Plates were normalized to an appropriate  $^3\text{H}$ -tissue standard of synthetic matrix (Amersham, Freiburg, Germany). Tritiated Pk11195 was also obtained from Amersham.  $^3\text{H}$ -CPFPX was obtained from the Institute of Neuroscience and Biophysics 4 (INB-4) at Research Centre Juelich.

### Tumour segmentation and size quantification

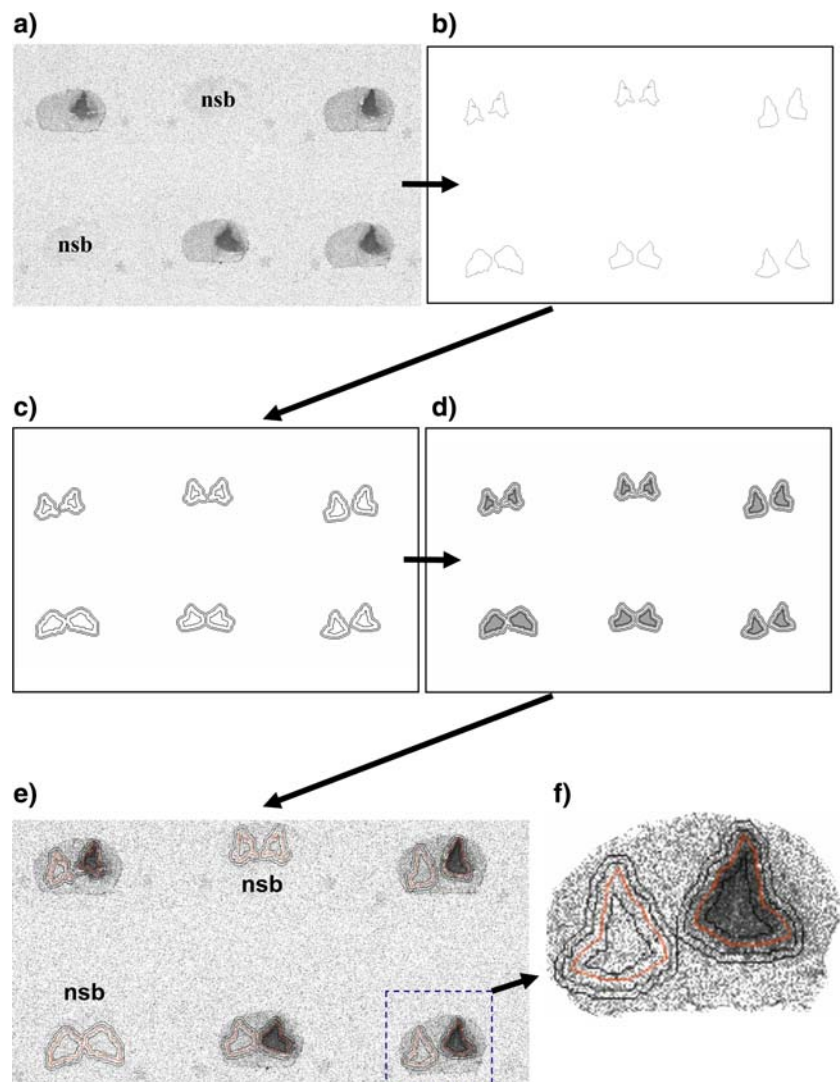
#### Delineation

The solid tumour mass was manually delineated within the  $^3\text{H}$ -Pk11195 autoradiographs [14] using the AIDA<sup>®</sup> software (Raytest, Straubenhardt, Germany). The segments were the basis for the automatic determination of adjacent tumour zones (Fig. 2).

#### Propagation

Following the tumour delineation in Pk slices, the segments were then transferred onto the adjacent  $^3\text{H}$ -CPFPX-radio-labelled slices by slice-segmentation and transfer together with the computed zones.

**Fig. 2** Segmentation work flow in AIDA<sup>®</sup> software. The autoradiographic film containing the dark labelled tumour regions from  $^3\text{H}$ -Pk11195 shown in (a) is either manually or automatically segmented (b). This contour is used for computing three different regions: the  $-300\ \mu\text{m}$  tumour zone, the  $300\ \mu\text{m}$  peritumoural zone and the  $600\ \mu\text{m}$  peritumoural zone (c). These contours are overlaid on the primary segmented tumour (d). Finally, these regions are back-projected onto the primary autoradiographic film (e). A single slice (dotted line) is enlarged in (f) with the primary tumour labelled by a red line. The non-specific binding slices are also segmented on the basis of the tumour contour of the adjacent slice for later background correction. *Abbreviations:* nsb, non specific binding



### Size quantification

The size of the tumours was determined on the basis of the  $25 \times 25 \mu\text{m}$  pixel resolution of the receptor autoradiographic film images, the  $20 \mu\text{m}$  slice thickness and the appropriate position of the slices in space. Coronal slices were numbered consecutively starting with the first slice in the telencephalic hemispheres.

Every fourth slice was radiolabelled with  $^3\text{H}$ -P<sub>k</sub>11195 and the slices in between were interpolated in order to make a quantitative assessment of the tumour size. The same procedure was applied for missing slices.

### Slice segmentation

Software was developed to separate the slice from the background. Neither the slice nor the noisy background constitutes a clear peak within the image histogram. Hence, histogram thresholding is not sufficient for slice segmentation. We used an iterative  $K_{\text{means}}$  algorithm [15] to determine the intensity ranges of a predefined number of clusters. The clusters representing low values are merged thus yielding a label image. The slice is detected as the largest of the connected components of the label image. The slice segments restrict the tumour adjacency zones.

### Determination of zones adjacent to the tumours

For an analysis of the various physiological zones within and around the tumours, three regions were determined: an inner tumour zone directed  $300 \mu\text{m}$  inwards from the outer tumour border, and two outer tumour zones, one from the outer tumour border to  $300 \mu\text{m}$  ( $300 \mu\text{m}$  peritumoural zone) and the second beginning at  $300 \mu\text{m}$  from the tumour to  $600 \mu\text{m}$  from the tumour ( $600 \mu\text{m}$  peritumoural zone). The different regions were computed following the segmentation of the tumour area and the slice on the basis of a Danielsson distance map [12]. The width of the zones is user-defined with respect to the original image resolution of  $25 \mu\text{m} \times 25 \mu\text{m}$  of the imaging film (Fig. 2c). The zones around the tumour that reach the brain surface have been omitted.

### Transfer of tumour zones onto $^3\text{H}$ -CPFPX-labelled slices

The propagation of the tumour segments (section ‘‘Image acquisition’’) to  $^3\text{H}$ -CPFPX allows the tumour zones to be transferred automatically. Only directly adjacent slices were used. To obtain an internal control, the regions from the bearing-bearing hemisphere were projected onto the contra-lateral hemisphere (Fig. 2d–f).

### Determination of receptor density

The amount of pBR and A<sub>1</sub>AR in fMol/mg protein ( $R_T$ ) was calculated from the amount of protein in wet weight ( $R_L$ ) determined from the tissue standard, the binding constant  $K_D$ -value of  $4.4 \text{ nM}$  and  $1.0 \text{ nM}$  of tritiated ligand for A<sub>1</sub>AR and P<sub>k</sub>11195, respectively, and the free activity  $F$  (determined from counting of the incubation solution) in the binding assay by  $R_T = R_L \times (K_D + F)/F$ .

Quantitative analysis was performed to average the respective region of each slice of a single tumour and also of all the tumours investigated. Quantification of analytical data was done by employing a Bas reader and AIDA software (Raytest, Straubenhardt, Germany). Plates were normalized to an appropriate  $^3\text{H}$ -tissue standard of synthetic matrix (Amersham, Freiburg, Germany).

### 3D reconstruction and visualization

The fully automatic 3D reconstruction procedure consists of multiple rigid registration steps. Starting at the middle of the P<sub>k</sub>11195 image stack, adjacent P<sub>k</sub>11195-labelled images are transformed according to optimum rotation and translation parameters maximizing the similarity of the images. Similarity was measured using the normalized correlation metric [16] and optimized by an iterative gradient descent optimizer with regular step length [17].

To achieve more robust results, the slices were first segmented (see section ‘‘Tumour segmentation and size quantification’’). Therefore, the similarity calculation was restricted to the slice area itself. Restacking yielded a consistent 3D data set without correction of non-rigid deformations (see Discussion). The transformation parameters of the slices were transferred onto the manual tumour segments and, hence, onto the adjacent zones.

The 3D reconstruction yields several consistent data sets containing original P<sub>k</sub>11195 values, tumour and slice labels, and tumour zones with P<sub>k</sub>11195 and CPFPX mean values. All these data sets were visualized using the Amira software (Mercury computer systems Inc., San Diego, CA, USA). Within this software package, the label data were used to visualize the slice and the tumour location. Superimposing the P<sub>k</sub>11195 and CPFPX zonal values allows their distribution around the tumour to be identified. To facilitate the examination, the data were enlarged by factor 4 in the Z direction.

### Statistics

Statistics was calculated with Graph-Pad prism software. One-way ANOVA with the Newman-Keuls post-test was used to compare different groups of animals. A  $p$ -value

< 0.05 was considered to be significant and  $p < 0.01$  was considered to be highly significant.

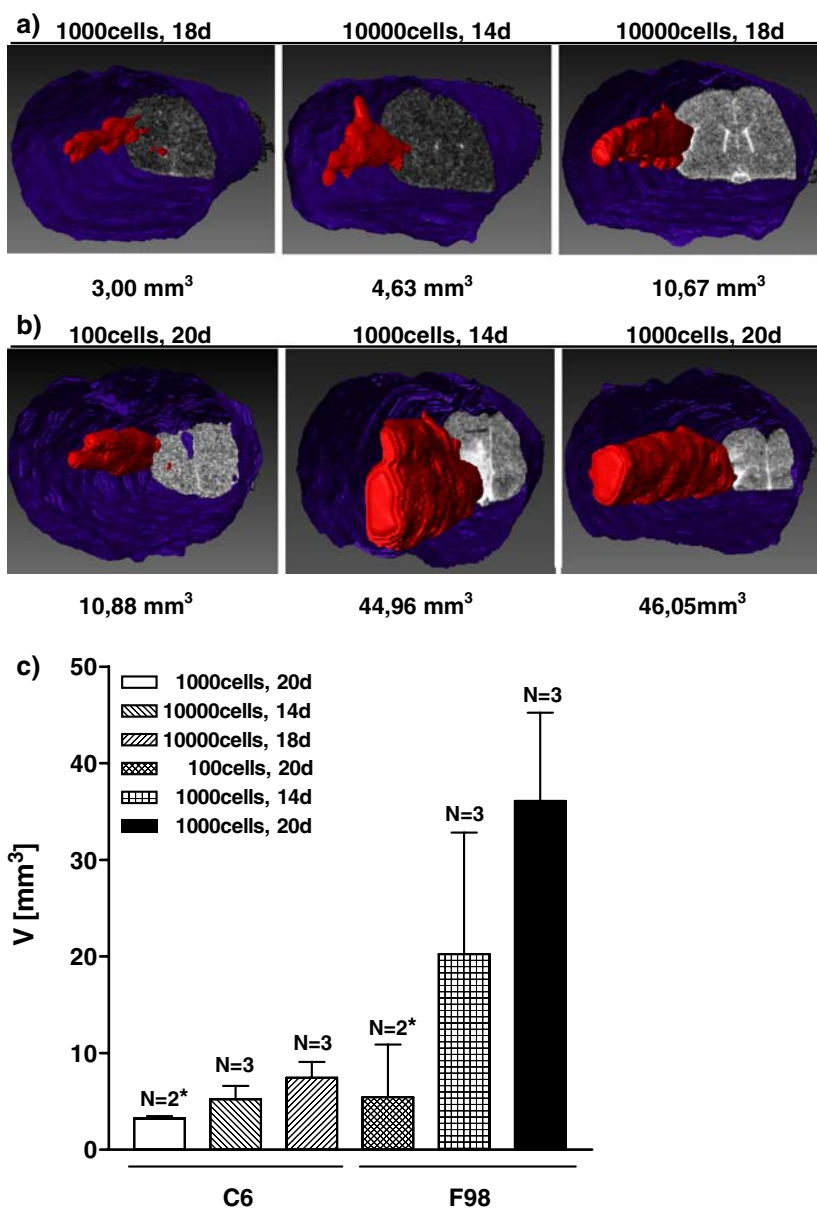
**Results**

Dependency of tumour size on numbers of implanted cells

Of 51 animals inoculated with a tumour (either F98 or C6), 17 were reconstructed to yield a consistent 3D tumour model. C6-tumours showed considerably slower growth characteristics compared to F98, as shown by typical examples in Fig. 3.

From double-determinations, 100 implanted cells (F98) grew to a tumour of  $10.88 \text{ mm}^3$  in one animal and no tumour in the second (mean = 5,441). In contrast, 1000 F98 cells implanted showed more consistent growth characteristics. Within 14 days, 1000 cells grew into tumours whose volume varied between  $20.25 \pm 21.77 \text{ mm}^3$  ( $N = 3$ ) and within 20 days to  $36.08 \pm 15.86 \text{ mm}^3$  ( $N = 3$ ). There were cases where the tumour grew to a size whose diameter completely filled the hemisphere and displaced the other hemisphere. Nevertheless, the animals showed no alteration in behaviour nor weight loss compared to controls assessed daily. In C6 animals, 1000 cells were tested, giving rise to a tumour of  $3.24 \pm 0.34 \text{ mm}^3$  within 20 days ( $N = 2$ ),

**Fig. 3** Dependency of tumour volume on numbers of implanted cells. Of 51 animals inoculated with a tumour, 17 were reconstructed yielding a consistent 3D tumour model. C6 tumours (a) showed considerably slower growth characteristics compared to F98 (b), as shown by typical examples. The respective volumes of the tumour examples shown are indicated below each picture. The summary of volumetric measurements is shown in (c). These have been evaluated on the basis of autoradiographic labelling of the pBR (see also part methods)



and from 10000 implanted cells tumours of  $5.21 \pm 2.39 \text{ mm}^3$  (14 d,  $N = 3$ ) and  $7.46 \pm 2.83 \text{ mm}^3$  (18 d,  $N = 3$ , value  $\pm$  SD, Fig. 3). From these characteristics, C6 tumours are estimated to grow ~40–50 times slower than equivalent numbers of implanted F98 cells.

#### Quantitative assessment of the dependency of receptor expression (pBR) on time of tumour development

Following the determination of the appropriate kinetics of tumour growth, systematically 10000 C6 or 1000 F98 tumour cells were inoculated and grew for different time intervals of either 10, 14, 18 or 20 days, respectively.

The time dependency of pBR expression in C6- and F98- tumours is shown in Fig. 4. With increasing duration of tumour development time, the pBR increases nearly exponentially in the tumours in vivo in the C6 model from  $0.085 \pm 0.05$  ( $N = 4$ ) in controls, via  $0.149 \pm 0.093$  (10 d,  $N = 3$ ),  $0.193 \pm 0.028$  (14 d,  $N = 5$ ),  $0.257 \pm 0.065$  (18 d,  $N = 4$ ) to  $0.402 \pm 0.325$  (20 d,  $N = 4$ , pMol/mg protein, values  $\pm$  SD), whereas there is a somewhat step-like increase in the F98 model. In the latter, from  $0.011 \pm 0.015$  in controls ( $N = 4$ ), the pBR-expression increased via  $0.402 \pm 0.099$  (10 d,  $N = 4$ ),  $0.704 \pm 0.502$  (14 d,  $N = 3$ ) and  $0.450 \pm 0.127$  (18 d,  $N = 3$ ) to  $0.572 \pm 0.031$  pMol/mg protein (20 d,  $N = 3$ , values  $\pm$  SD).

#### Various zones around the tumours: dependency of receptor-expression ( $A_1AR$ ) on time of tumour development

The next step in the investigation was to assess the  $A_1AR$  expression over the time of tumour development.

Therefore, tumour cells of either the C6 or the F98 cell line were tested for the presence of  $A_1AR$ -messenger RNA (m-RNA) before implantation (Fig. 5a). Furthermore,  $A_1AR$  expression was assessed autoradiographically in various zones in and around C6 and F98 tumours as a function of time of tumour development (Fig. 5b). RT-PCR from mRNA derived from rat glioma cell lines F98 and C6 (lanes 1 and 2) or total rat brain (RB1, RB2, lanes 3 and 4) of two different animals, showing that tumour cells do not express  $A_1AR$  prior to inoculation.

Neither C6 nor F98 cells (Table 1) express  $A_1AR$  in culture. Although there is virtually no  $^3H$ -CPFPX binding within the tumour area as determined from receptor autoradiography,  $A_1AR$  is present to some extent, with 110 to 150 fMol/mg in C6 and around 85 to 95 fMol/mg in F98 tumours. During the period of tumour growth, the overall  $A_1AR$  expression in the vicinity of the tumour was more or less stable in the C6 model, with  $152.35 \pm 87.04$  fMol/mg on day 10 in the C6 model to  $298.72 \pm 40.10$  fMol/mg on day 14,  $183.26 \pm 86.64$  fMol/

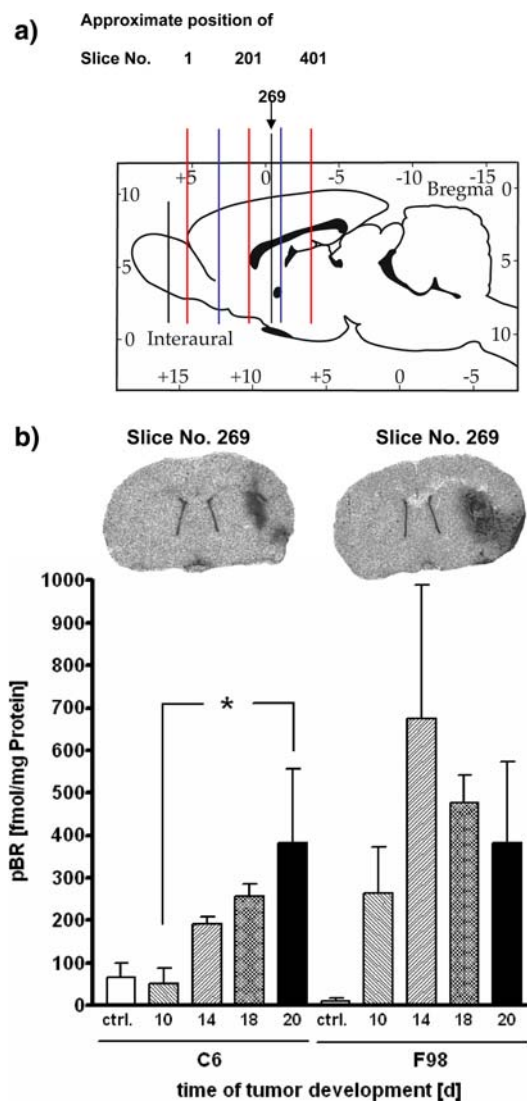
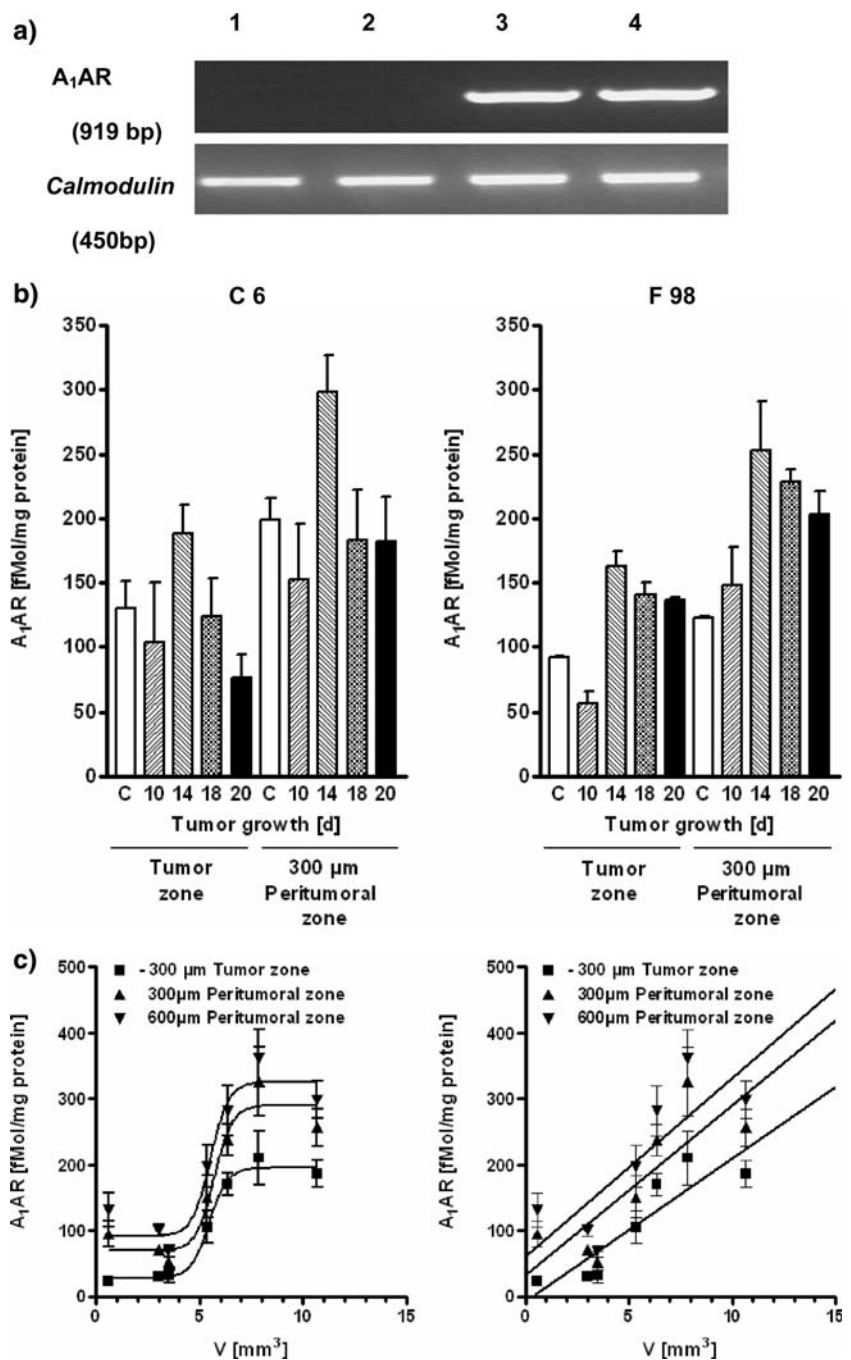


**Fig. 4** Dependency of pBR—expression on time of tumour development. (a) Schematic drawing of a sagittal view from Paxinos and Watson rat brain atlas [18] is shown with slice numbers 1–401 and their approximate location in the various brain nuclei or landmarks. Slice counting of the coronal 20  $\mu$ m cryoslices started with the first slice in the telencephalic hemispheres indicated by '1'. Position of slice 1, 201 and 401 are indicated by red lines (from left to right). Positions of slice 101 and 301 are indicated by blue lines, respectively. (b) Receptor autoradiographs with pBR ligand  $^3H$ -Pkl1195 on cryo-slices from 10000 C6 or 1000 F98 tumour cells in the  $-300 \mu$ m Tumour zone [values  $\pm$  SD]. The cells were inoculated and grew for either 10, 14, 18 or 20 days. A one-way ANOVA with Newman-Keuls post-test showed that in the C6 model the pBR expression 10 d versus 20 d is significant ( $p < 0.05$ ) indicated by an asterisk, whereas other intervals are not. Above the bar chart, a representative pBR autoradiographic slice (number '269') is shown for a C6 (left) and an F98 animal (right), respectively

mg and  $182.52 \pm 68.99$  fMol/mg. In contrast, it increased significantly in the F98 model from  $147.77 \pm 58.98$  fMol/mg on day 10, via  $253.06 \pm 65.78$  fMol/mg on day 14 and  $228.91 \pm 16.33$  fMol/mg on day 18 to  $203.39 \pm 25.68$  fMol/mg on day 20 in the F98 model,



**Fig. 5** Dependency of A<sub>1</sub>AR expression on time of tumour development in various zones of both (C6 and F98) tumour models. **(a)** RT-PCR with cDNA derived from rat glioma cell lines (F98, C6) before implantation or total rat brain (RB1, RB2) obtained from two different animals is shown in the upper trace as an example. **(b)** Dependency of A<sub>1</sub>AR expression on time of tumour development. A<sub>1</sub>AR expression was assessed in various zones in and around F98 (right) and C6 tumours (left) as a function of time of tumour development. **(c)** Furthermore, for both rat tumour models the A<sub>1</sub>AR expression was computed against the volume of the tumour entity. In C6 tumours an interrelation between A<sub>1</sub>AR growth and tumour size is found, which suggests that sigmoidal curve fitting is the best mathematical description. Left: sigmoidal curve fitting without variable slope (Hill coefficient = 1). For comparison, the linear fit is shown on the right with parameters as indicated. In F98 animals, no correlation exists between F98 A<sub>1</sub>AR and tumour volume ( $r^2 = 0.0027$ ,  $r^2 = 0.1519$ ,  $r^2 = 0.1965$ , for -300  $\mu$ m tumour zone, 300  $\mu$ m Peritumoural zone and 600  $\mu$ m Peritumoural zone, and with a slope of 0.055, 0.536 and 0.672, respectively. A sigmoidal fit did not converge in these cases (not shown)



respectively, as determined from the receptor autoradiographs (values  $\pm$  SD). The amount of A<sub>1</sub>AR only increased significantly in the peritumoural zone in a manner dependent on the time of tumour development in the F98 model with  $p < 0.05$  between 10 d versus 14 d and of attenuated cells versus 14, 18, and 20 days, respectively. Furthermore, in the tumour itself, following an initial decrease of A<sub>1</sub>AR at 10 d ( $p < 0.01$  versus attenuated control and  $p < 0.001$  versus 14, 18 and 20 days), the A<sub>1</sub>AR presence rose to a plateau from 14 and 18 d to 20 days, probably due to invading cells from the immune system or periphery or due

to ‘wrapping’ of normal tissue astrocytes or neurons by tumour cells (see also Discussion). In the C6 animals, neither within the tumour entity nor in the surrounding 300  $\mu$ m peritumoural zone was any significant increase of A<sub>1</sub>AR detected over time.

Dependency of A<sub>1</sub>AR presence on tumour volume

The interdependence of A<sub>1</sub>AR expression on tumour size was assessed, without regard to number of implanted cells or time of tumour development (Fig. 5c).

**Table 1** Summary of all groups investigated with manually segmented and automatically reconstructed tumour zones (values  $\pm$  SD)

	C	10	14	18	20
<b>C6-cells</b>					
<i>10,000 cells</i>					
pBR [fMol/mg]	85.55	149.01	193.46	256.71	402.2
$\pm$ SD (N)	53.92 (4)	93.37 (4)	28.38 (3)	64.97 (5)	324.89 (4)
A <sub>1</sub> AR [fMol/mg] <sup>a</sup>	129.90	103.64	188.23	124.18	75.77
$\pm$ SD (N)	43.73 (4)	92.76 (4)	31.72 (2)	65.88 (5)	37.45 (4)
A <sub>1</sub> AR [fMol/mg] <sup>b</sup>	199.41	152.35	298.72	183.26	182.52
$\pm$ SD (N)	32.02 (4)	87.04 (4)	40.10 (2)	86.64 (5)	68.99 (4)
V [mm <sup>3</sup> ]	n.d.	n.d.	4.63	6.35	3.00*
			3.17	5.34	3.48*
			7.85	10.67	0.57
V [mm <sup>3</sup> ]			5.22	7.45	n.d.
$\pm$ SD			2.39 (3)	2.83 (3)	
<b>F98-cells</b>					
<i>1000 cells</i>					
pBR [fMol/mg]	10.65	401.56	704.16	450.12	572.19
$\pm$ SD (N)	15.45 (4)	99.47 (4)	502.14 (3)	127.31(3)	31.16 (2)
A <sub>1</sub> AR [fMol/mg] <sup>a</sup>	91.68	56.28	163.09	140.20	136.51
$\pm$ SD (N)	3.39 (4)	18.70 (4)	20.28 (3)	17.84 (3)	2.60 (2)
A <sub>1</sub> AR [fMol/mg] <sup>b</sup>	123.13	147.77	253.06	228.91	203.39
$\pm$ SD (N)	1.44 (4)	58.98 (4)	65.78 (3)	16.33 (3)	25.68 (2)
V [mm <sup>3</sup> ]	n.d.	n.d.	20.25	36.08	10.88**
$\pm$ SD (N)			21.77 (3)	15.86 (3)	

\* 20 days, 1000 cells

\*\* 20 days, 100 cells

<sup>a</sup> -300  $\mu$ m tumour zone<sup>b</sup> 300  $\mu$ m peritumoural zone

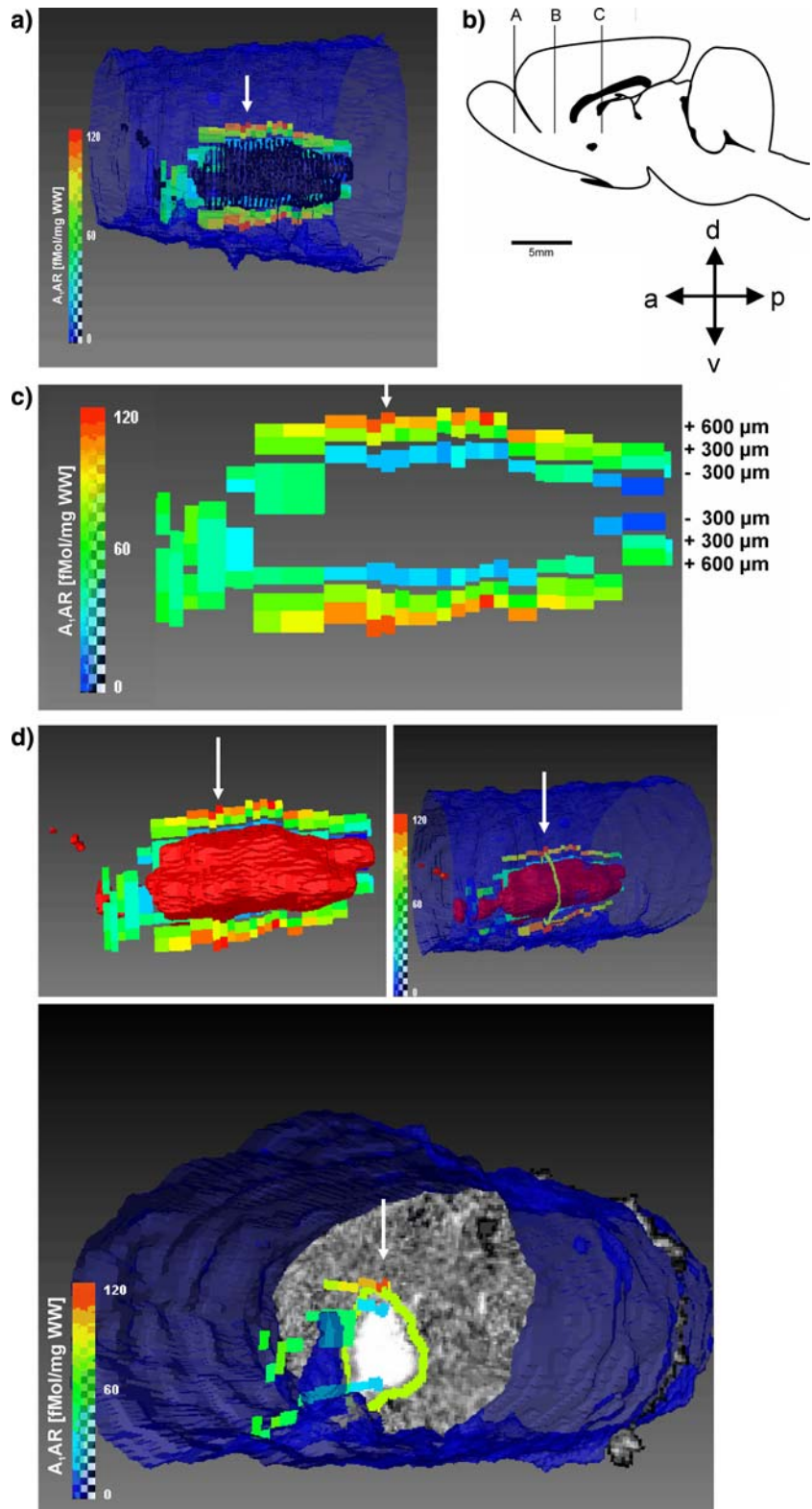
Therefore, values of A<sub>1</sub>AR [fMol/mg protein] calculated from laboratory standards where plotted against tumour size from 3D tumour reconstruction and fitted with non-linear regression (sigmoidal dose-response with and without variable slope, and comparing two models of the fit) and in a second approach the values were fitted with a linear regression. Both models clearly suggested, that there is a non-linear dependency of A<sub>1</sub>AR presence and tumour size. For the C6 model, this dependency is strikingly sigmoidal with a goodness of fit greater than 99%. In the F98 model, this dependency is clearly not sigmoidal and not linear. Here, the best approach for describing the curve is the two-site competition model.

Dependency of receptor expression (A<sub>1</sub>AR, pBR, 3D) in various zones around tumours on time of tumour development. Rostro-caudal differences in A<sub>1</sub>AR expression?

Finally, coronal cryosliced tumour brains were analyzed to estimate possible alterations in A<sub>1</sub>AR expression around

tumours in various microenvironments (such as rostral part of the basal ganglia with naturally comparably low A<sub>1</sub>AR expression level versus the hippocampal formation with very high amounts of A<sub>1</sub>AR in the oriental layer (stratum oriens) and molecular layer (stratum moleculare). Beginning with the first containing-containing slice, all <sup>3</sup>H-CPFPX slices were colour-coded, yielding an overall lateral view of the tumour permitting rostro-caudal alterations to be estimated. A 3D-representation of the solid tumour (dark) and two aural zones around it are given in Fig. 6a. The scale on the left-hand side ranges from 0 to 120 fMol/mg. On the right trace, a schematic drawing from a rat brain (18) is shown with the appropriate tumour area indicated (Fig. 6b). A lateral view of the aura around the isolated tumour is shown in (Fig. 6c). The scale reflects the values in the various zones of the tumour. The thin space in between the aura zones marks the outer border of the tumour. Note: The A<sub>1</sub>AR expression is higher towards the aura of the middle part of the tumour entity and decreases towards the ends. In (Fig. 6d) the lateral (upper trace) or coronal view (lower trace) of a tumour is provided as an

**Fig. 6** Receptor-expression ( $A_1AR$ , pBR, 3D) in various zones around single tumour entities and rostro-caudal differences in  $A_1AR$  expression. **(a)** Lateral view with the complete 3D tumour view and the aural zones is shown as an example. The tumour of approximately  $10\text{ mm}^3$  is shown with the  $300\ \mu\text{m}$  and the  $600\ \mu\text{m}$  zone around it. In the more central part of the tumour where the diameter is larger,  $A_1AR$  expression is also clearly higher. **(b)** Schematic lateral view of an entire rat brain is shown with the following levels indicated: (A) first slice counted, (B) first slice containing tumour, (C) end-slice of tumour. Scale bar: 5 mm, orientation bar: a anterior, p posterior, d dorsal v ventral. **(c)** The three zones around the tumour as indicated by  $+300\ \mu\text{m}$ ,  $+600\ \mu\text{m}$  and  $-300\ \mu\text{m}$  without the tumour itself displayed. Scale bar to the left indicates the quantity of  $A_1AR$  in the various zones of the tumour in fMol/mg wet weight ranging from 0 to 120 fMol/mg. **(d)** Finally, three examples of options for visualization by AMIRA software are presented. The colour-coded bar represents quantities of  $A_1AR$  at each position in space. Note: One ring around the tumour is quantitatively the average of the  $300\ \mu\text{m}$ -peritumoural zone (or  $-300\ \mu\text{m}$  or  $600\ \mu\text{m}$  zone, respectively) at this entire level around the tumour. Therefore, the aura above and below the tumour is indicated by the same colour since it represents the same averaged region of the autoradiographic slice. The white arrows indicate the same position on each slide



example. For better contrast, the tumour entity itself is shown in red.

Finally, the reconstructed 3D images were re-transferred onto the schematic Paxinos and Watson atlas and the  $A_1AR$

distribution was observed in the  $300\ \mu\text{m}$  invasion zone in context of various microenvironments (Fig. 7).

The following regions were accordingly assigned: slice 1–101 prefrontal, 102–201: caudate putamen, 202–301:

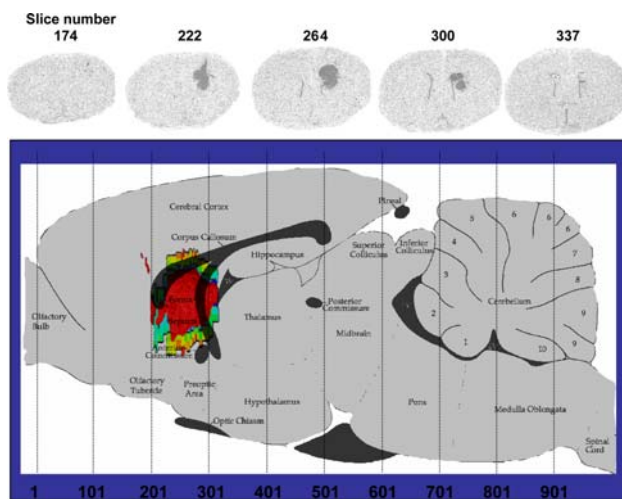


**Fig. 7** Retrocession of 3D reconstructed images onto the schematic Paxinos/ Watson Atlas. As an example, one tumour was re-projected into the schematic Paxinos and Watson sagittal view

corpus callosum/ fornix/ anterior commissure and 302–401 fornix/ thalamus/ hippocampus. In four different C6 animals (10000 cells, 18 days), a drop in  $A_1AR$  expression in the first outer tumour zone at the beginning of the thalamus - around slice 320 has been found (not shown).

## Discussion

### Summary of results

In the present paper, we describe a quantitative analysis of the spatial distribution of functional receptor proteins in 2D and 3D in various zones of tumour entities in rat brain glioma models.

Experimentally, we provide evidence that expression of  $A_1AR$  in C6 tumours is merely dependent on the tumour volume rather than on number of implanted cells or time of tumour growth.

Methodologically, we used *in vitro* imaging techniques and developed image processing software for fully automatic 3D reconstruction and peri-tumoural zone computation. The software allows the seamless processing of the output with standard commercial autoradiography and visualization software.

The method developed by us yielded quantitative results with respect to various growth zones of the tumour as well as rostro-caudal differences of tumour growth in various microenvironments.

The influence of different microenvironments on tumour growth is delineated in comparison to the contra-lateral hemisphere.

With this method we show that growth characteristics of allogenic C6 tumours in Wistar rats compared to syngeneic

F98 cells implanted into Fisher F344 rat brains is about 40–50 times slower.

The volume of C6 tumours varies between 3 and 10 mm<sup>3</sup> following implantation of 10,000 cells during a tumour growth period of 10–18 days.

For comparison, F98 tumours grow to sizes of 10–46 mm<sup>3</sup> in a comparable schedule, despite only 1000 cells being implanted.

It was shown that with time of tumour development, pBR density within and  $A_1AR$  in the outer zones around the tumours increases in both models. The latter seem to correlate with necroses occurring within the tumour entity. The first registration step yields reliable results. Nevertheless, since no ground truth is available for our images, errors might occur which also affect the coherent segmentation of the tumour volume.

### Methodological discussion, possible biases

With increasing tumour size necroses might occur. This enucleation makes it difficult to map the specific binding of radiolabelled ligands within the tumour (especially Pk11195 [13]).

The tumour volume calculation is occasionally biased due to lost slices and slice shrinkage during preparation. Nevertheless, this is not a specific problem for automatic processing. We propose the interpolation of the missing or shrunk slices by non-linear image matching of the adjacent Cresyl-violet slices or by external *in vivo* references such as CT, MRI or combined *in vivo/ex vivo* approaches such as PET with subsequent autoradiography.

Here, following cryoslicing, adjacent slices were subjected to different staining protocols, including <sup>3</sup>H-Pk11195 and <sup>3</sup>H-CPFPX receptor autoradiography. The two protocols are at least in part performed with solutions at pH 7.6 (Pk11195 protocol) or pH 7.4 (CPFPX protocol), respectively. Therefore, tissue shrinkage was found to differ slightly (for reference and example see: [19]). Furthermore, during the tissue processing procedure, after cryoslicing the slices are dried on a 33°C heating plate for 30 min and in a stream of cold air. These processes might alter the slice spreading and thus could have an impact on relative size of tumour reconstruction following receptor autoradiography compared to non-invasive techniques such as PET.

In a few cases, the tumour-bearing hemisphere was enlarged. Therefore, segmented regions could not have been projected onto the contra-lateral hemisphere as control. Tumours grown rostrally especially near the olfactory node also invaded very lateral areas and contacted the borders of the brain. This made the determination of 300 μm or even 600 μm peritumoural zones impossible. Therefore, in the cases where the tumour grew that later-

ally, the 300 and 600  $\mu\text{m}$  peritumoural zones were omitted and reoriented, and the only complete segmented tumours are those grown centrally in the respective hemispheres, otherwise as indicated.

Other techniques yielding information about tumour size and position

Tumour volume estimation and reconstruction is necessary for various experimental approaches: for example, effectiveness of pharmacological treatment (e.g. [20, 21]), assessment and monitoring of angiogenesis [4], or post-surgical histological characterization [5]. Furthermore, there is an obvious need for fast and exact tumour localization plus a margin of safety from non-invasive techniques especially during surgery. Other techniques might yield information about the sizing of tumours. Among these, besides positron emission tomography (PET), magnet resonance tomography (MRT), computer tomography (CT), single photon emission computer tomography (SPECT), mention should be made of intravital microscopy [4] or other fluorescent-optical techniques as non-invasive and non-radioactive techniques. In non-invasive imaging techniques such as PET and MRT, voxel resolution is by far more insensitive (e.g. in small animal PET and MRT: 10–100 times, PET: approximately  $1.4 \times 1.4 \times 1.6 \text{ mm}^3$ , MRT:  $1.0 \times 1.0 \times 1.2 \text{ mm}^3$ ) compared to receptor autoradiographic techniques (25  $\mu\text{m}$  isotropic resolution). The differences in the resolution limits of these various imaging techniques as well as real tissue borders and functional nuclei imply that the most sensitive techniques (like receptor autoradiography) are not those with which the brain is imaged in its natural position, but those that have the best resolution for reconstruction.

Positioning of findings within published results

Monitoring the  $A_1AR$  expression and receptor presence around experimentally implanted tumours has been shown to be of value since this receptor system has been described as being up-regulated during the cerebral response to glioma invasion in GBM and thus can serve as a marker for the peritumoural zone in primary human GBM [1]. To our knowledge, increased  $A_1AR$  expression in solid tumours has so far only been described in human GBM and human colon cancer [1, 8].

Among the events during tumour growth that might lead to increased  $A_1AR$  expression identified to date is the possible presence of the pro-stimulatory cytokine IL-6, which up-regulates  $A_1AR$  on glial cells in low-level  $A_1AR$ -expression areas and rat brain slices [22].

As shown recently [7], the size of the tumour can influence IL-6 and also IL-1 secretion (in human pituitary

adenoma), and this, in turn, has been shown to induce  $A_1AR$  expression around tumours [22] and VEGF [7].

Without a supply of new blood vessels the size of a tumour can only reach a volume of about  $2 \text{ mm}^3$  as diffusion of oxygen can occur at a distance of just 100–200  $\mu\text{m}$  [23].

The sizes of the tumours assessed from 3D reconstruction are within the ranges that have been described by other groups in various implantation models, e.g. by Yang et al. [3], Vajkoczy et al. [4], Zhang et al. [24], Sun et al. [25] or Bhujwala et al. [26].

No study yet focusing upon gene expression profiles in human GBM (e.g. [2, 3, 27]) has described an alteration in  $A_1AR$  expression within tissue. A reason might be that besides an up-regulation of  $A_1AR$  in the peritumoural zone of GBM, there is a tendency for  $A_1AR$  to decrease within the tumour itself as well as in the outer tumour area and oedema zone, and a roughly 100-fold decrease of  $A_1AR$  in GBM cell lines (unpublished data, manuscript in preparation).

This might imply that, whenever possible, detected candidate genes or proteins in GBM of relevance for invasivity, growth behaviour or malignancy should also be assessed spatially with autoradiographic or histological techniques.

Understanding the growth of tumours means mapping out and modelling the topological and dynamical properties of cells in their respective microenvironment [28]. Comparing implantation models of various cell lines and various animal strains, it seems obvious that the size and dynamics of tumour growth depends on the number of implanted cells and, moreover, on the local environment in which the tumour grows [4, 5, 24, 25]. Thus, a tool at hand for looking at the tumour zones, the tumour microenvironment as well as alterations in the native surrounding tissue is clearly required.

Based upon the quantified tumour in a 3D representation and the  $25 \mu\text{m} \times 25 \mu\text{m}$  pixel resolution of the autoradiographic imaging technique, we furthermore determined and quantified zonal density and alterations over time of tumour development for pBR and  $A_1AR$ . This might also be of use for comparison with non-invasive imaging techniques like PET. A thorough evaluation of this method is necessary taking into consideration all experimental influences. Overall, by applying this new image processing tool in combination with pharmacological results, we will obtain a valuable estimation of brain tumour growth in rats.

During tumour growth, besides invading stem cells from the bone marrow [29] and neuronal precursor cells [30], the settlement and persistence of calcium-channel inhibitor-sensitive cancer stem cell-like subpopulations has been described, which might also influence the peritumoural microenvironment composition [31].

From the growth characteristics it might be speculated that in contrast to the ENU-induced F98 tumour, as C6 cells induce an immune response, since there is no syngeneic host available [32, 33], that invading B- and T-cells might slow down the effective net tumour growth.

The possibility of 3D in situ analysis of alterations in tumour tissue will enable the study of the microenvironment in and around tumours with respect to proteins, DNA expression and elements by receptor autoradiography, in situ hybridization and mass spectrometry (e.g. LA-ICP-MS), respectively. All these different techniques yield images that might be combined to multimodal 3D visualizations of zones in and around tumours.

The importance of assessing the microenvironment has been demonstrated for various characteristics of tumours such as invasivity [34–37], motility and mitosis [3, 38], neo-vascularization, and flow dynamics [4, 39] or receptor protein rearrangement [38]. The formation of secondary tumours and protein expression such as CD 44 might also depend on the microenvironment [32, 40, 41].

A<sub>1</sub>AR which has been found to be up-regulated in the peritumoural zone of high-grade gliomas [1] has also been found to exert an influence on tumour cell migratory motility [42].

## Summary and conclusion

Understanding alterations in the tumour cell microenvironment and occurring interactions during tumour growth as well as techniques that link non-invasive imaging to gene- or receptor-expression will help to better understand tumour pathology and develop treatment options that are adapted onto the tumour development. A multimodal assessment of tumour development will also lead to reduced numbers of experimental animals.

## References

- Bauer A, Langen KJ, Bidmon H, Holschbach MH, Weber S, Olson RA, Coenen HH, Zilles K (2005) <sup>18</sup>F-Cyclopentyl-3-(3-<sup>18</sup>F-Fluoropropyl)-1-Propyl-xanthine PET identifies changes in cerebral A<sub>1</sub>Adenosine receptor density caused by glioma invasion. *J Nucl Med* 46:450–454
- Hoelzinger DB, Mariani L, Woyke T, Berens TJ, McDonough WS, Sloan A, Coons SW, Berens M (2005) Gene expression profile of glioblastoma multiforme invasive phenotype points to new therapeutic targets. *Neoplasia* 7(1):7–16
- Liyang Y, Diehn M, Watson N, Bollen AW, Aldape KD, Nicholas MK, Lamborn KR, Berger MS, Botstein D, Brown PO, Israel MA (2005) Gene expression profiling reveals molecularly and clinically distinct subtypes of glioblastoma multiforme. *Proc Natl Acad Sci USA* 102(16):5814–5819
- Vajkoczy P, Schilling L, Ullrich A, Schmiedek P, Menger MD (1998) Characterization of angiogenesis and microcirculation of high-grade glioma: an intravital multicolor fluorescence microscopic approach in the athymic nude mouse. *J Cereb Blood Flow Metab* 18:510–520
- Wesseling P, Van der Laak JAWM, De Leeuw H, Ruiters DJ, Burger PC (1994) Quantitative immunohistological analysis of the microvasculature in untreated human glioblastoma multiforme; computer-assisted image analysis on whole tumour sections. *J Neurosurg* 81:902–909
- Acker T, Acker H (2004) Cellular oxygen sensing need in CNS functions: physiological and pathological implications. *J Exp Biol* 207:3171–3188
- Borg SA, Kerry KE, Royds JA, Battersby RD, Jones TH (2005) Correlation of VEGF production with IL1a and IL6 secretion by human pituitary adenoma cells. *Eur J Endocrinol* 152:293–300
- Khoo HE, Ho CL, Chatwal VJS, Chan STF, Ngoi SS, Mochhala SM (1996) Differential expression of adenosine A<sub>1</sub> receptors in colorectal cancer and related mucosa. *Cancer Lett* 106:17–21
- Ralevic V, Burnstock G (1998) Receptors for purines and pyrimidines. *Pharm Rev* 50(3):413–492
- Barth RF (1998) Rat brain tumour models in experimental neuro-oncology: the 9L, C6, T9, F98, RG2 (D74), RT-2 and CNS-1 Gliomas. *J Neurooncol* 36:91–102
- Benda P (1968) Differentiated rat glial cell strain in tissue culture. *Science* 161:370–371
- Danielson PE (1980) Euclidean distance mapping. *Comput Graphics Image Process* 14:227–248
- Miyazawa N, Hamel E, Diksic M (1998) Assessment of the peripheral benzodiazepine receptors in human gliomas by two methods. *J Neurooncol* 38:19–26
- Jordà EG, Jiménez A, Verdaguer E, Canudas AM, Folch J, Sureda FX, Camins A, Pallàs M (2005) Evidence in favour of a role for peripheral-type benzodiazepine receptor ligands in amplification of neuronal apoptosis. *Apoptosis* 10:91–104
- Duda RO, Hart PE (1973) Pattern classification and scene analysis. *J Wiley & Sons, New York, USA*
- Kim J, Fessler JA (2004) Intensity-based image registration using robust correlation coefficients. *IEEE Trans Med Imag* 23(11):1430–1444
- Ibanez L, Schroeder W, Ng L, Cates J (2005) The ITK software guide, 2nd edn. <http://www.itk.org>
- Paxinos G, Watson C (1986) The rat brain in stereotaxic coordinates. *Academic Press, Sydney*
- Palm C, Dehnhardt M, Vieten A and Pietrzyk U (2005) 3D rat brain tumour reconstruction. Proceedings of 14th International Conference of IOMP, EFOMP and DGMP (ICMP 2005) and of 39th Annual Congress of DGBMT within VDE (BMT 2005). Kalender W, Hahn EG, Schulte AM (eds) *Biomedizinische Technik* 50(1):597–598
- Bifulco M, DiMarzo V (2002) Targeting the endocannabinoid system in cancer therapy: a call for further research. *Nat Med* 8(6):547–550
- Kirsch M, Schackert G, Black PMcL (2000) Anti-angiogenic treatment strategies for malignant brain tumours. *J Neurooncol* 50:149–163
- Biber K, Lubrich B, Fiebich BL, Boddeke HWGM, von Calker D (2001) Interleukin-6 enhances expression of Adenosine A<sub>1</sub> receptor mRNA and signalling in cultured rat cortical astrocytes and brain slices. *Psychopharmacol* 24:86–96
- Dulak J, Józkwicz A (2005) Anti-angiogenic and anti-inflammatory effects of statins: relevance to anti-cancer therapy. *Curr Cancer Drug Targets* 5(8):579–594
- Zhang Y, Zhao W, Zhang HJ, Domann FE, Oberley LW (2002) Over-expression of copper zinc superoxide dismutase suppresses human glioma cell growth. *Cancer Res* 62:1205–1212
- Sun Y, Schmidt NO, Schmidt K, Doshi S, Rubin JB, Mulkern RV, Carroll R, Ziu M, Erkmen K, Poussaint TY, Black P, Albert

- M, Burstein D, Kieran MW (2004) Perfusion MRI of U87 brain tumours in a mouse model. *Magn Res Med* 51:893–899
26. Bhujwala ZM, Artemov D, Natarajan K, Ackerstaff E, Solaiyappan M (2001) Vascular differences detected by MRI for metastatic versus nonmetastatic breast and prostate cancer xenografts. *Neoplasia* 3:143–153
  27. Denko NC, Fontana LA, Hudson KM, Sutphin PD, Raychaudhuri S, Altman R, Giaccia AJ (2003) Investigating hypoxic tumour physiology through gene expression patterns. *Oncogene* 22:5907–5914
  28. Bredel M, Bredel C, Juric D, Harsh GR, Vogel H, Recht LD, Sikic BI (2005) Functional network analysis reveals extended gliomagenesis pathway maps and three novel MYC-interacting genes in human gliomas. *Cancer Res* 65(19):8679–8689
  29. Tabatabai G, Bähr O, Möhle R, Eyüpoglu IY, Boehmler AM, Wischhusen J, Rieger J, Blümcke I, Weller M, Wick W (2005) *Brain* 128:2200–2211
  30. Glass R, Synowitz M, Kronenberg G, Walzlein JH, Markovic DS, Wang LP, Gast D, Kiwit J, Kempermann G, Kettenmann H (2005) Glioblastoma-induced attraction of endogenous neural precursor cells is associated with improved survival. *J Neurosci* 25(10):2637–2646
  31. Kondo T, Setoguchi T, Taga T (2004) Persistence of a small subpopulation of cancer stem-like cells in the C6 glioma cell line. *Proc Natl Acad Sci USA* 101(3):781–786
  32. Grobbs B, De Deyn PP, Slegers H (2002) Rat C6 glioma as experimental model system for the study of glioblastoma growth and invasion. *Cell Tissue Res* 310:257–270
  33. Parsa AT, Chakrabarti I, Hurley PT, Chi JH, Hall JS, Kaiser MG, Bruce JN (2000) Limitations of the C6/Wistar rat intracerebral glioma model: implications for evaluating immunotherapy. *Neurosurgery* 47(4):993–1000
  34. Belién ATJ, Paganetti P, Schwab ME (1999) Membrane-type 1 matrix metalloprotease (MT1-MMP) enables invasive migration of glioma cells in central nervous system white matter. *J Cell Biol* 144:373–384
  35. Koderá T, Nakagawa T, Kubota T, Kubota M, Sato K, Kobayashi H (2000) The expression and activation of matrix metalloproteinase-2 in rat brain after implantation of C6 rat glioma cells. *J Neurooncol* 46:105–114
  36. Estève PO, Tremblay P, Houde M, St-Pierre Y, Mandeville R (1998) In vitro expression of MMP-2 and MMP-9 in glioma cells following exposure to inflammatory mediators. *Biochim Biophys Acta* 1403:85–96
  37. Senner V, Sturm A, Baur I, Schrell UHM, Distel L, Paulus W (1999) CD 24 promotes invasion of glioma cells in vivo. *J Neuropathol Exp Neurol* 58(8):795–802
  38. Nishikawa R, Ji XD, Harmon RC, Lazar CS, Gill GN, Cavenee WK, Su Huang HJ (1994) A mutant epidermal growth factor receptor common in human glioma confers enhanced tumorigenicity. *Proc Natl Acad Sci USA* 91:7727–7731
  39. Vajkoczy P, Menger MD (2000) Vascular microenvironment in gliomas. *J Neurooncol* 50:99–108
  40. Pilkington GJ, Akinwunmi J, Ognjenovic N, Rogers JP (1993) Differential binding of anti-CD44 on human gliomas in vitro. *Neuroreport* 4:259–263
  41. Koshyomn S, Penar P, Wadsworth MP, Taatjes DJ (1997) Localization of CD44 at the invasive margin of glioblastomas by immunoelectron microscopy. *Ultrastruct Pathol* 21:517–525
  42. Woodhouse EC, Amanatullah DF, Schetz JA, Liotta LA, Stracke ML, Clair T (1998) Adenosine receptor mediates motility in human melanoma cells. *Biochem Biophys Res Commun* 246:888–894